DALTON
FULL PAPER

Crystal structures and magnetic properties of mercury(II) bromide complexes with pyridyl-substituted *N*-oxyl *N*′-oxides (nitronyl nitroxides)

Chin-Jhan Lee,[a] Chian-Hong Huang,[a] Ho-Hsiang Wei,*[,a] Yi-Hung Liu,[b] Gene-Hsiang Lee[b] and Yu Wang[b]

[a] *Department of Chemistry, Tamkang University, Tamsui, Taiwan*
[b] *Instrumental Center, College of Science, National Taiwan University, Taipei, Taiwan*

The crystal structures have been determined and magnetic properties investigated for four novel $HgBr_2$ complexes with pyridyl-substituted 'nitronyl nitroxides', 4,4,5,5-tetramethyl-2-(4-pyridyl)-(L^1), -2-(2-pyridyl)-(L^2), -2-(3-pyridyl)-(L^3) and -2-(6-methyl-2-pyridyl)-2-imidazoline *N*[1]-oxyl *N*[3]-oxide (L^4). Complex **1**, $[HgBr_2L^1]$, is mononuclear, in which mercury(II) has planar trigonal co-ordination core, from two bromide atoms and one nitrogen atom of the pyridyl group. In **2**, $[HgBr_2L^2]$ the Hg^{II} atom has distorted-tetrahedral four co-ordination involving two bromide atoms and chelating by oxygen and nitrogen atoms of the L^2 ligand. Complex **3**, $[(HgBr)_3L^3{}_2]$, is a zigzag polymeric chain with a distorted T-shaped $HgBr_2L^3$ unit and self-assembly involving co-ordination by an oxygen atom of the nitroxide groups. Complex **4**, $[(HgBr_2)_3L^4{}_2]$, is a quasi-linear chain with $HgBr_2L^4$ moieties and $HgBr_2$ cores. Cryomagnetic susceptibility measurements (4–300 K) showed that **1** and **3** exhibit a weak intermolecular alternating one-dimensional antiferromagnetic exchange interaction, while **3** and **4** possess weak one-dimensional antiferromagnetic and ferromagnetic exchange interactions respectively. A simple spin-polarization model has been used to justify the observed ferromagnetic exchange interaction between the spins of the radical NO group in complex **4**.

The magnetic properties of a large number of stable organic *N*-oxyl *N*′-oxides (nitronyl nitroxides) and their metal complexes have been studied, especially in order to understand the factors that influence the magnetic exchange interactions between the metal ion and the radical centers.[1–4] Recently, several magnetic properties of pyridyl-substituted *N*-oxyl *N*′-oxide radicals[5–8] and their metal complexes[9–15] have been reported. These radicals are especially attractive due to their donor atoms and to assemble an extended co-ordination geometry with changing magnetic coupling.

Several transition-metal complexes with 4,4,5,5-tetramethyl-2-(4-pyridyl)-2-imidazoline *N*[1]-oxyl *N*[3]-oxide (L^1)[8,9] and a few metal complexes with 4,4,5,5-tetramethyl-2-(2-pyridyl)-2-imidazole *N*[1]-oxyl *N*[3]-oxide (L^2)[10] and 4,4,5,5-tetramethyl-2-(3-pyridyl)-2-imidazoline *N*[1]-oxyl *N*[3]-oxide (L^3)[11] have been studied. Although the different magnetic behaviours have been previously observed in these systems, however systematic studies of diamagnetic metal complexes with paramagnetic L^1–L^3 radical ligands have been lacking.

Accordingly, we report herein the structural characterization and magnetic properties of $HgBr_2$ complexes with the four related pyridyl-substituted radical ligands L^1–L^3 and 4,4,5,5-tetramethyl-2-(6-methyl-2-pyridyl)-2-imidazoline *N*[1]-oxyl *N*[3]-oxide (L^4). We will show that the shortest contacts involving the intermolecular hydrogen bonding and the bridging bromides of $HgBr_2$ are appropriate crystalline design elements with which to control the crystal packing and also to generate antiferromagnetic or ferromagnetic exchange interactions and to propagate them along predetermined spatial directions.

Experimental

Syntheses

The pyridyl-substituted radicals L^1–L^4 were prepared and purified according to the methods reported.[16,17] The complexes $[HgBr_2L^1]$ **1**, $[HgBr_2L^2]$ **2**, $[(HgBr_2)_3L^3{}_2]$ **3** and $[(HgBr_2)_3L^4{}_2]$ **4** were prepared in the same manner as follows. To a solution of $HgBr_2$ (0.2 mmol) in ethanol (10 cm^3) was added with stirring a solution of the radical (0.2 mmol) in ethanol (10 cm^3). The solution was stirred for an additional period then allowed to stand at room temperature for several days. Crystals suitable for X-ray crystallographic analysis were obtained and filtered off (Found: C, 24.4; H, 2.8; N, 7.0. Calc. for $C_{12}H_{16}Br_2HgN_3O_2$ **1**: C, 24.3; H, 2.7; N, 7.1. Found: C, 24.1; H, 2.7; N, 7.0. Calc for $C_{12}H_{16}Br_2HgN_3O_2$ **2**: C, 24.2; H, 2.7; N, 7.1. Found: C, 18.5; H, 2.7; N, 5.4. Calc. for $C_{24}H_{32}Br_6Hg_3N_6O_4$ **3**: C, 18.6; H, 2.1; N, 5.4. Found: C, 23.2; H, 3.0; N, 6.0. Calc. for $C_{26}H_{36}Br_6Hg_3N_6O_4$ **4**: C, 23.4; H, 3.0; N, 6.0%). IR (KBr disc): $\tilde{\nu}_{NO}/cm^{-1}$ 1369 (**1**), 1368 (**2**), 1366 (**3**) and 1365 (**4**).

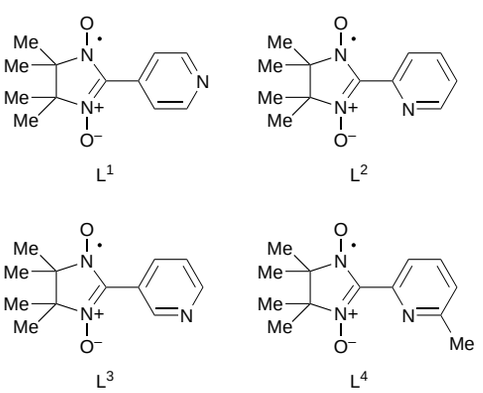

Physical measurements

The IR spectra were recorded on a Bio-Rad FTS40 FTIR spectrophotometer as KBr pellets in the 400–4000 cm^{-1} region, X-band EPR spectra at 300 K for the complexes as powders on a Bruker ESC-106 spectrometer. The temperature dependence of the magnetic susceptibility of the polycrystalline samples was measured between 4 and 300 K at field 1 T using a

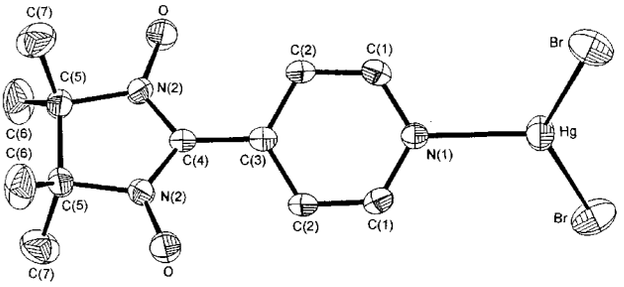

Fig. 1 Perspective view of complex **1** with the atom numbering scheme. Thermal ellipsoids are drawn at the 30% probability level

Quantum Design model MPMS computer-controlled SQUID magnetometer. Diamagnetic corrections were made using Pascal's constants.[18]

Crystallography

Crystal data. *Complex* **1** $C_{12}H_{16}Br_2HgN_3O_2$. $M = 594.67$, monoclinic, space group $C2/c$, $a = 11.3272(20)$, $b = 14.174(3)$, $c = 10.132(3)$ Å, $\beta = 104.038(16)°$, $U = 1578.1(6)$ Å^3, $Z = 4$, $D_c = 2.503$ g cm^{-3}, $F(000) = 1088$, $\mu = 147.714$ cm^{-1}, crystal size = 0.25 × 0.30 × 0.50 mm, $2\theta_{max} = 55.0°$, $N = 1813$, $N_o = 1463$, $R = 0.031$, $R' = 0.036$.

Complex **2**. $C_{12}H_{16}Br_2HgN_3O_2$, $M = 594.67$, monoclinic, space group $P2_1/c$, $a = 10.5811(12)$, $b = 22.038(4)$, $c = 7.2584(9)$ Å, $\beta = 103.858(13)°$, $U = 1643.3(5)$ Å^3, $Z = 4$, $D_c = 2.404$ g cm^{-3}, $F(000) = 1088$, $\mu = 141.854$ cm^{-1}, crystal size = 0.20 × 0.20 × 0.40 mm, $2\theta_{max} = 50.0°$, $N = 2895$, $N_o = 1788$, $R = 0.039$, $R' = 0.039$.

Complex **3**. $C_{24}H_{32}Br_6Hg_3N_6O_4$, $M = 1551.75$, orthorhombic, space group *Pbca*, $a = 7.643(3)$, $b = 20.886(5)$, $c = 22.733(4)$ Å, $U = 3629.2(16)$ Å^3, $Z = 4$, $D_c = 2.840$ g cm^{-3}, $F(000) = 2771$, $\mu = 128.466$ cm^{-1}, crystal size = 0.15 × 0.20 × 0.50 mm, $2\theta_{max} = 50.0°$, $N = 3184$, $N_o = 1969$, $R = 0.060$, $R' = 0.055$.

Complex **4**. $C_{26}H_{36}Br_6Hg_3N_6O_4$, $M = 1577.79$, monoclinic, space group $P2_1/c$, $a = 10.958(6)$, $b = 24.663(9)$, $c = 7.339(4)$ Å, $\beta = 102.29(5)°$, $U = 1937.9(16)$ Å^3, $Z = 2$, $D_c = 2.704$ g cm^{-3}, $F(000) = 1414$, $\mu = 120.316$ cm^{-1}, crystal size = 0.05 × 0.30 × 0.40 mm, $2\theta_{max} = 45.0°$, $N = 2581$, $N_o = 1542$, $R = 0.066$, $R' = 0.067$.

The X-ray crystal data were collected at room temperature using an Enraf-Nonius CAD4 diffractometer equipped with graphite-monochromated Mo-Kα radiation (λ = 0.7107 Å), 2θ–θ scan mode. The N independent reflections and N_o with $I > 2.0\sigma(I)$ were observed. The structures were solved by location of heavy atoms using a Patterson map and refined by a full-matrix least-squares method using the NRCVAX[19] software package; the function minimized was $\Sigma w(|F_o| - |F_c|)^2$, where $w = 1/\sigma^2(F_o)$. All non-hydrogen atoms were readily located and refined with anisotropic thermal parameters; $R = \Sigma||F_o| - |F_c||/\Sigma|F_o|$ and $R' = (\Sigma w|F_o - F_c|^2/\Sigma|F_o|^2)^{\frac{1}{2}}$.

CCDC reference number 186/771.

Results and Discussion

IR and EPR spectra

The most important infrared absorption bands of complexes **1**–**4** at 1369, 1368, 1366, and 1365 cm^{-1} respectively have been assigned to the N–O stretching mode. The EPR (9.7–9.80 GHz) spectra at 300 K in benzene solution all consisted of five lines centred at $g = 2.01$, with nitrogen hyperfine coupling constants $a^N = 7.56$, 7.48, 7.67, and 7.45 G respectively (G = 10^{-4} T).

Crystal structures

The crystal structure of $[HgBr_2L^1]$ **1** is illustrated in Fig. 1. The mercury atom has a distorted trigonal three-co-ordination comprised of two terminal bromide atoms and the pyridyl nitrogen atom of L^1 with Hg–Br 2.4666(9) Å, Br–Hg–Br 134.73(4)°, and Hg–N(1) 2.292(8) Å (Table 1). The fragment O–N(2)–C(4)–N(2)–O [N(2)–O 1.296(7) Å] is coplanar as expected due to orbital conjugation and as shown by the sum of the angles of the bonds around the N(2) and C(4) atoms. The unit cell (Fig. 2) contains two pairs of symmetrically related molecules of the $[HgBr_2L^1]$ with tail-to-tail (units of I and II), head-to-tail (II and III), and tail-to-head (III and IV) alternating arrangements along the b axis. Thus the two different intermolecular NO groups of the L^1 radicals are far apart: 4.623(10) (between units II and III) and 5.142(12) Å (between I and II). It is noteworthy that the shortest intermolecular (between II and III) contact is NO···HC(1′) 2.633 Å.

Table 1 Selected bond distances (Å) and angles (°) for $[HgBr_2L^1]$ **1**

Hg–Br	2.4666(9)	Hg–N(1)	2.292(8)
N(2)–O	1.296(7)	C(4)–N(2)	1.335(8)
Br–Hg–Br	134.73(4)	Br–Hg–N(1)	112.64(3)
C(1)–N(1)–Hg	120.8(4)	C(1)–N(1)–C(1)	118.3(7)
C(4)–N(2)–O	125.4(6)	N(2)–C(4)–N(2)	109.0(7)
C(5)–N(2)–O	121.5(5)		

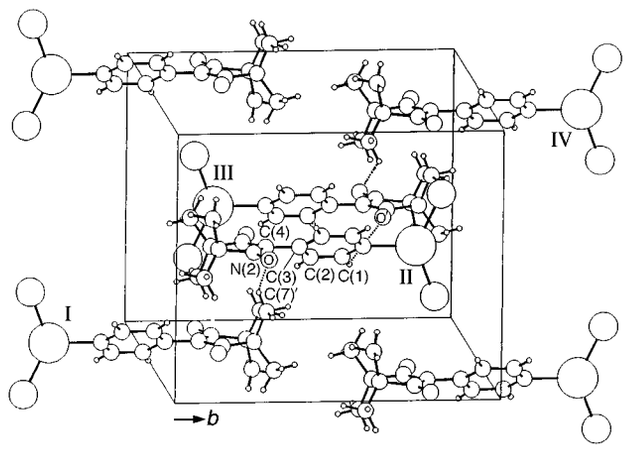

Fig. 2 View of the packing of the molecules in complex **1**. Weak intermolecular hydrogen bonds are shown by dotted lines

The structure of $[HgBr_2L^2]$ **2** is shown in Fig. 3. Four-co-ordination of Hg^{II} is formed by two terminal bromide atoms [Hg–Br(1) 2.4412(17), Hg–Br(2) 2.4397(18) Å, and Br(1)–Hg–Br(2) 162.05(7)°] and one oxygen and one nitrogen atom from the L^2 ligand [Hg–O(1) 2.521(9), Hg–N(1) 2.666(11) Å, O(1)–Hg–N(1) 68.3(3)°] in a distorted tetrahedral geometry (Table 2). The fragment O(1)–N(2)–C(6)–N(3)–O(2) with the co-ordinated N(2)–O(1) 1.281(13) Å and the unco-ordinated N(3)–O(2) 1.268(14) Å is nearly planar but forms a dihedral angle of 38.1(4)° with the plane of the pyridyl ring. From the unit-cell packing (Fig. 4), two pairs of symmetrically related molecules of $[HgBr_2L^2]$ are arranged tail-to-tail and head-to-head and tail-to-tail along the b axis. The shortest intermolecular contact between the O(2) atom of the N(2)–O(2) group and the hydrogen atom, H(10′), of the methyl group [C(10′)H$_3$] in neighbouring molecules forms a weak hydrogen bond N(2)O(2)···H(10)C(1′) 2.330(9) Å. The head-to-head intermolecular distance Hg···Br(2′) is 3.4340(20) Å. The shortest intermolecular contact O(2)···O(2′) between the NO groups is 3.661(3) Å.

The structure of complex **3** consists of two crystallographically independent units, $HgBr_2$ and $[(HgBr_2)_2L^3_2]$. As shown in Fig. 5, each Hg(2) atom is co-ordinated by two bromide atoms [Hg(2)–Br(2) 2.4520(22), Hg(2)–Br(3) 2.4441(21) Å] and a nitrogen atom from a pyridyl moiety [Hg(2)–N(1) 2.452(13) Å] in a distorted fashion (Table 3). The self-assembly bonding with O(1) of the nitroxide group [Hg(2)–O(1) 2.655(13) Å] extends

Table 2 Selected bond distances (Å) and angles (°) for $[HgBr_2L^2]$ **2**

Hg–Br(1)	2.4412(17)	Hg–Br(2)	2.4397(18)
Hg–O(1)	2.521(9)	Hg–N(1)	2.666(11)
N(2)–O(1)	1.281(13)	N(3)–O(2)	1.268(14)
Br(1)–Hg–Br(2)	162.05(7)	Br(1)–Hg–O(1)	97.35(21)
O(1)–Hg–N(1)	68.6(3)	Br(2)–Hg–O(1)	100.24(21)
Br(2)–Hg–N(1)	97.0(3)	Br(1)–Hg–N(1)	92.69(24)
Hg–O(1)–N(2)	114.1(7)	Hg–N(1)–C(5)	127.2(8)
Hg–N(1)–C(1)	117.1(9)		

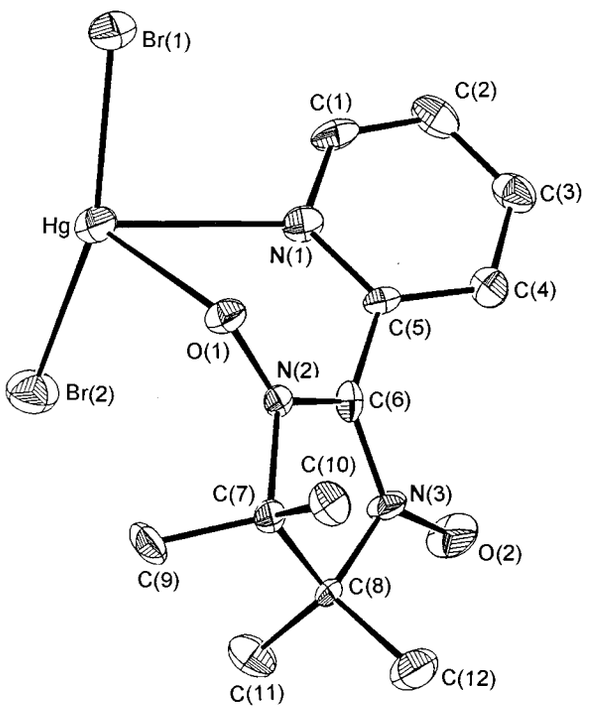

Fig. 3 Perspective view of complex **2**. Details as in Fig. 1

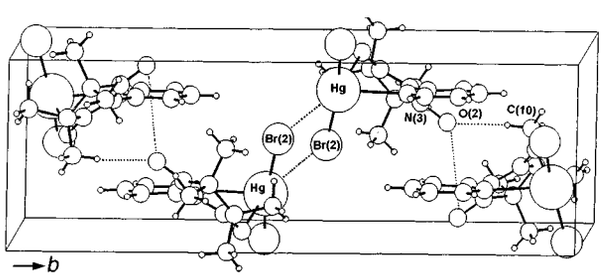

Fig. 4 View of the packing of the molecules in complex **2**. Details as in Fig. 2

the co-ordination number of Hg(2) to four, forming a zigzag polymeric chain. The O(1)–N(2)–C(6)–N(3)–O(2) moiety is as expected coplanar, but forms a dihedral angle of 33.8(6)° with the plane of the pyridyl ring. The shortest contact distances O(2′)···O(2′) and O(2)···H(10′) between atoms belonging to different L^3 ligands are 3.8223(14) and 2.329(17) Å respectively, which can be considered as weak interactions.

The crystal structure of complex **4** as shown in Fig. 6 consists of two co-ordination types for Hg^{II}. The Hg(2) atom has a distorted-tetrahedral co-ordination by virtue of chelating O(2) and N(1) atoms of ligand L^4 and two terminal Br(3) and Br(2) atoms. Atom Hg(1), originally co-ordinated by two bromides, has a linear co-ordination [Br(1)–Hg(1)–Br(1) 179.9°, Hg–Br(1) 2.446(3) Å], Table 4, and additional weak bonds to four bromide atoms, two Br(3) and two Br(2) atoms, from neighbouring $Hg(2)Br_2$ moieties; thus, there is six-co-ordination about Hg(1), leading to a chain-like motif in the structure. The fragment O(1)–N(2)–C(7)–N(3)–O(2) is nearly planar, but forms a

Table 3 Selected bond distances (Å) and angles (°) for $[(HgBr_2)_3L^3_2]$ **3**

Hg(2)–Br(2)	2.4520(22)	Hg(2)–Br(3)	2.4441(21)
Hg(2)–N(1)	2.452(13)	Hg(2)–O(1)	2.655(13)
N(2)–O(1)	1.263(19)	N(3)–O(2)	1.27(3)
Hg(1)–Br(1)	2.4156(21)		
Br(2)–Hg(2)–Br(3)	160.34(7)	Br(1)–Hg(1)–Br(1)	180.0
Br(3)–Hg(2)–O(1)	86.7(3)	Br(3)–Hg(2)–N(1)	96.4(4)
Br(2)–Hg(2)–O(1)	102.4(3)	N(1)–Hg(2)–O(1)	88.2(4)
C(6)–N(2)–O(1)	127.0(16)	C(7)–N(2)–O(1)	120.8(13)

Table 4 Selected bond distances (Å) and angles (°) for $[(HgBr_2)_3L^4_2]$ **4**

Hg(1)–Br(1)	2.446(3)	Hg(2)–Br(2)	2.448(3)
Hg(2)–Br(3)	2.450(4)	Hg(2)–O(2)	2.460(4)
Hg(2)–N(1)	2.628(17)	N(3)–O(2)	1.27(3)
N(2)–O(1)	1.30(3)	Hg(1)···Br(2)	3.108(3)
Hg(1)···Br(3)	3.280(4)		
Br(1)–Hg(1)–Br(1)	179.9	Br(2)–Hg(2)–Br(3)	164.38(13)
Br(2)–Hg(2)–O(2)	101.2(5)	Br(3)–Hg(2)–N(1)	94.3(5)
Br(2)–Hg(2)–N(1)	97.5(4)	Br(2)–Hg(2)–O(2)	92.0(5)
N(3)–O(2)–Hg(2)	109.6(17)	N(1)–Hg(2)–O(2)	72.8(7)
C(7)–N(3)–O(2)	129.4(22)	C(7)–N(2)–O(1)	125.8(23)

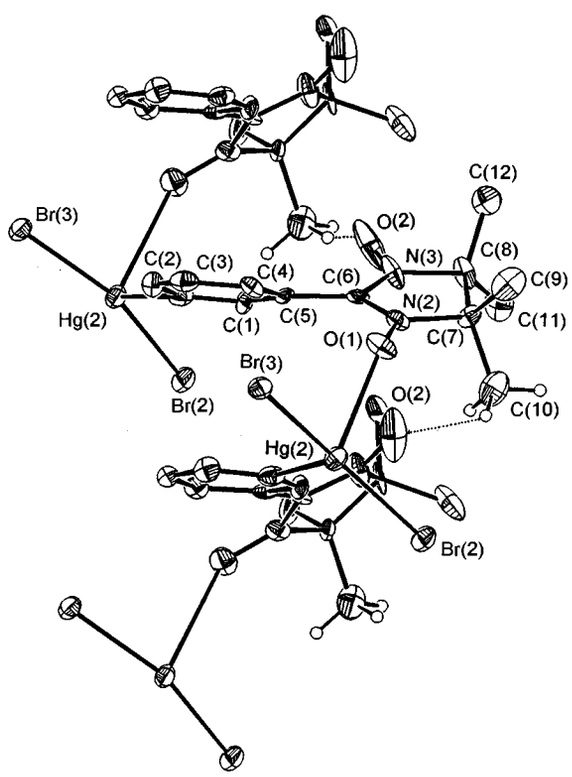

Fig. 5 Perspective view of complex **3** with the atom numbering scheme. Atoms Hg(1) and Br(1) are omitted for clarity. Thermal ellipsoids are drawn at the 30% probability level. Weak interligand hydrogen bonds are drawn as dotted lines

dihedral angle of 43.0(8)° with the plane of the pyridyl ring. The shortest contact distances, C(12)H···O(1′) and O(1)···O(1′), belonging two different L^4 radicals, are 2.663(21) and 3.7785(10) Å respectively.

In summary, the shortest contact distances O···H, belonging to two different radicals, in complexes **1**–**4** are 2.633(6), 2.330(9), 2.329(17), and 2.663(21) Å respectivley, which are close to the sum of the van der Waals radii (2.6 Å).

Magnetic properties

The $\chi_m T$ *vs.* T plots for complexes **1**–**4** are shown in Fig. 7 in the 4–300 K range. The $\chi_m T$ value at 300 K of **1**, 0.36 cm^3 K mol^{-1},

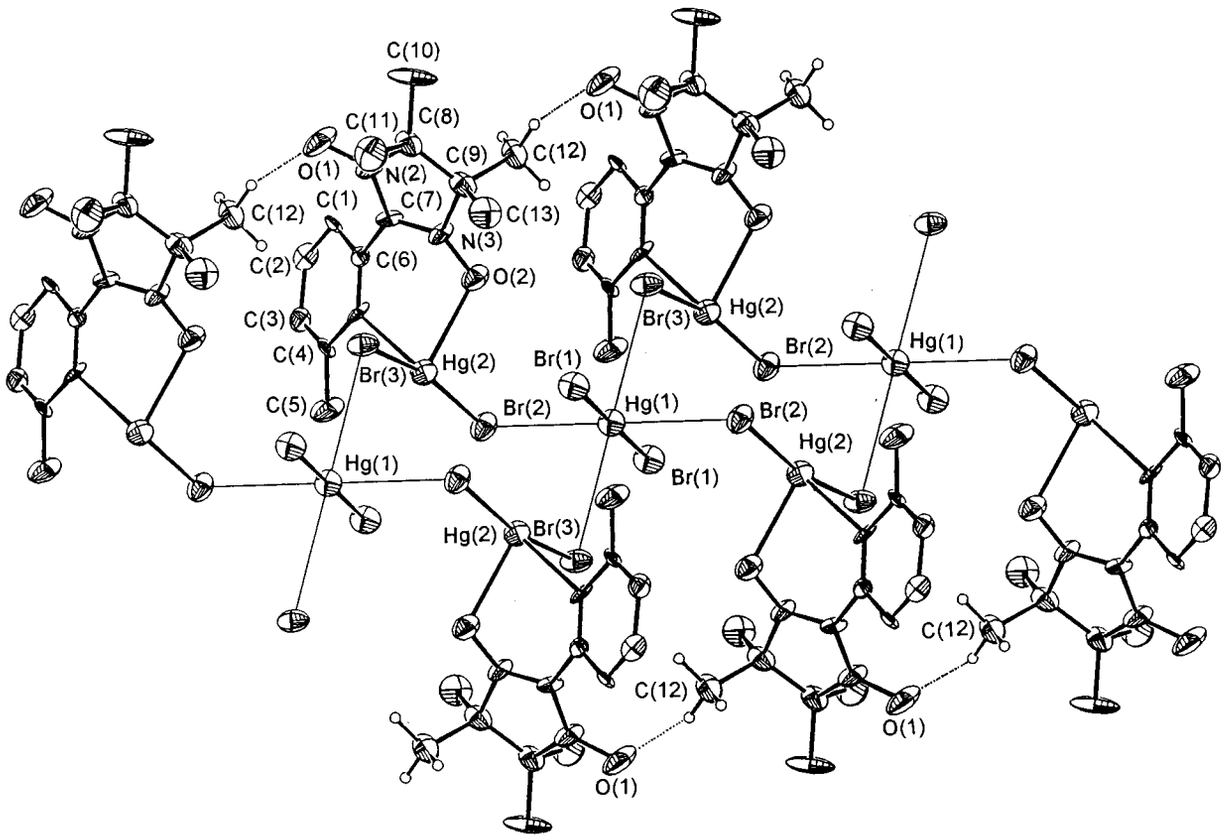

Fig. 6 Perspective view of complex **4** with the atom numbering scheme. Thermal ellipsoids are drawn at the 30% probability level. Weak intermolecular hydrogen bonds are drawn as dotted lines

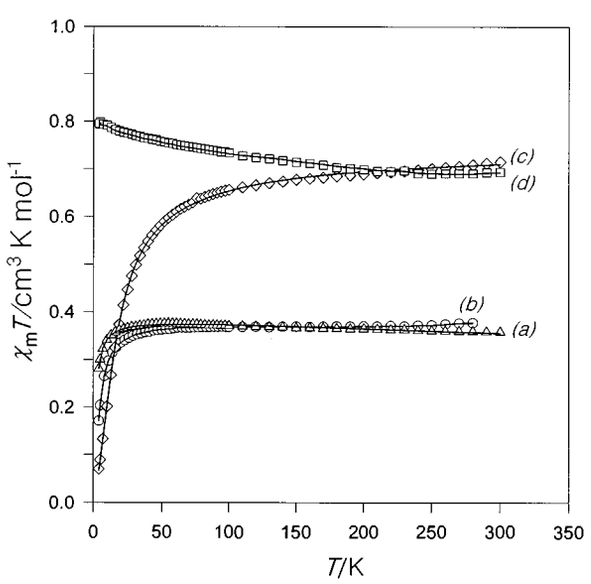

Fig. 7 Temperature dependence of $\chi_m T$ for complexes **1** (*a*), **2** (*b*), **3** (*c*), and **4** (*d*). The solid lines are calculated with the parameters reported in the text

is close to the value expected for non-coupled spins $S = \frac{1}{2}$ (0.375 cm^3 K mol^{-1}), increases slowly with decreasing temperature reaching a maximum at about 50 K, then decreases rapidly on further lowering of temperature. This is characteristic of a weak antiferromagnetic exchange interaction in **1**. Clearly, the magnetic interaction does not arise from the diamagnetic mercury(II) ions. The structural analysis of **1** shows that the unit cell contains alternating pairs of $[HgBr_2L^1]$ radicals with two different intermolecular distances involving NO groups. Consequently, the magnetic data were analysed by use of the expression (1) for the exchange coupling in an alternating chain

$$\chi_m = (Ng^2\mu_B^2/kT)[(A + Bx + Cx^2)/(1 + Dx + Ex^2 + Fx^3)] \quad (1)$$

of $S = \frac{1}{2}$ ion developed by Hall *et al.*[20] where $x = J/kT$, $A = 0.25$, $B = 0.125\,87 + 0.227\,52\alpha$, $C = 0.019\,111 - 0.133\,07\alpha + 0.5967\alpha^2 - 1.3167\alpha^3 + 1.0081\alpha^4$, $D = 0.107\,72 + 1.4192\alpha$, $E = -0.002\,852\,1 - 0.4236\alpha + 22.1953\alpha^2 - 0.824\,12\alpha^3$, and $F = 0.377\,54 - 0.067\,022\alpha + 0.9805\alpha^2 - 21.678\alpha^3 + 15.838\alpha^4$. The alternation parameter α is defined by the zero-field spin Hamiltonian (2) where J and αJ are the exchange interaction

$$H = -2J\sum_{i=1}^{n/2}(S_{2i}\cdot S_{2i-1} + \alpha S_{2i}\cdot S_{2i+1}) \quad (2)$$

parameters associated with a particular intermolecular spin interaction of NO groups between the units II and III and units I and II in the unit cell respectively. Since the data concern organic radicals, calculations did not include a contribution from the temperature-independent paramagnetism. A tolerable best fit obtained (the solid line in Fig. 7) with this equation leads to $J = -2.05$ cm^{-1}, $g = 2.01$ (from EPR spectroscopy), $\alpha = 0.10$ and $R = 2.1 \times 10^{-5}$. The discrepancy R value is defined as $\Sigma(\chi_m^{obs} - \chi_m^{calc})^2/(\Sigma\chi_m^{obs})^2$.

For compound **2** the $\chi_m T$ value at 280 K, 0.38 cm^3 K mol^{-1}, is identical to that expected for non-coupled spins $S = \frac{1}{2}$. On lowering the temperature $\chi_m T$ decreases slowly to reach a value of 0.33 cm^3 K mol^{-1} at 25 K, and then decreases rapidly to 0.17 cm^3 K mol^{-1} at 4 K. This suggests that the free radicals, L^2, in **2** have weak intermolecular antiferromagnetic coupling. On the basis of the structural results, the unit cell contains alternating differently spaced intermolecular nitroxide radicals, therefore the magnetic data were also fitted according to equation (1), giving $J = -2.47$ cm^{-1}, $g = 2.01$ (from EPR spectroscopy), $\alpha J = 0.35$ cm^{-1}, and $R = 5.3 \times 10^{-5}$, where J and αJ are the exchange interaction constants associated with a particular

intermolecular spin exchange of NO groups between the tail-to-tail and head-to-head aligned species respectively in the unit cell of **2**.

For compound **3** the $\chi_m T$ value at 300 K, 0.73 cm^3 K mol^{-1}, is slightly lower than that expected for a non-coupled spin $S = \frac{1}{2}$ system (0.75 cm^3 K mol^{-1}). On lowering the temperature $\chi_m T$ decreases rapidly and approaches 0.07 cm^3 K mol^{-1} at 4 K. This behaviour is characteristic of an intrachain antiferromagnetic exchange interaction between two NO$^\bullet$ radicals in this polymer chain. We have attempted to reproduce theoretically the experimental susceptibility in this zigzag polymeric regime by use of the published expression (3) for $J < 0$ calculated by Bonner and

$$\chi = (Ng^2\mu_B{}^2/kT)(A/B) \quad (3)$$

Fischer[21] for a classical-spin Heisenberg array of $S = \frac{1}{2}$ spins, where $x = J/kT$, $A = 0.25 + 0.074\,97x + 0.075\,235x^2$ and $B = 1.0 + 0.9931x + 0.172\,135x^2 + 0.747\,825x^3$. A very close agreement with the experimental data is obtained (the solid line in Fig. 7) with $J = -14.70$ cm^{-1}, $g = 2.01$ (from EPR spectroscopy) and $R = 2.0 \times 10^{-5}$.

For compound **4** the $\chi_m T$ value at 300 K, 0.71 cm^3 K mol^{-1}, is slightly lower than that expected for a non-coupled spin $S = \frac{1}{2}$ system. On lowering the temperature $\chi_m T$ increases slowly and approaches 0.81 cm^{-3} K mol^{-1} at 4 K which is higher than 0.75 cm^3 K mol^{-1} for a non-coupled spin $S = \frac{1}{2}$ system; thus it is indicative of a weak ferromagnetic exchange interaction between L^4 radicals in complex **4**. According to the structural results, this weak ferromagnetic behaviour is caused by an intermolecular interaction between two neighbouring NO$^\bullet$ radicals through CH · · · ON in this quasi-polymeric chain. To fit quantitatively the magnetic data for **4**, we first considered the exchange interaction as the leading term with the corresponding two spins $S_1 = S_2 = \frac{1}{2}$ of a Hamiltonian $H = -2JS_1S_2$. However, fitting the data with this model gave very poor results. Thus we used the empirical expression of the magnetic susceptibility proposed by Baker *et al.*[22] to fit ferromagnetic one-dimensional isotropic Heisenberg $S = \frac{1}{2}$ chains, equation (4)

$$\chi = [Ng^2\mu_B{}^2/4k(T - \theta)](N/D)^{\frac{2}{3}} \quad (4)$$

where $x = J/2kT$, $N = 1.0 + 5.797\,991\,6x + 16.902\,653x^2 + 29.376\,885x^3 + 29.832\,959x^4 + 14.036\,918x^5$ and $D = 1.0 + 2.797\,991\,6x + 7.008\,678\,0x^2 + 8.653\,864\,4x^3 + 4.574\,311\,4x^4$. The solid curve in Fig. 7 represents the best fit of the experimental data obtained with $J = 0.24$ cm^{-1}, $g = 2.01$ (from EPR spectroscopy), $\theta = 0.145$ K, and $R = 3 \times 10^{-4}$.

Since the fitted magnetic data of complex **4** provide evidence for a weak intermolecular ferromagnetic interaction, one must consider a possible mechanism for exchange interaction between the nearest-neighbour L^4 radicals. From the structural and the magnetic results discussed above, there is a weak intermolecular contact between the NO groups [O(1) · · · O(1′) 3.7785(10) Å]. Such a NO · · · ON′ contact means a direct intermolecular exchange interaction between the magnetic orbitals, however it is usually considered responsible for weak antiferromagnetic coupling in molecular solids.[23] An acceptable mechanism suggested by McConnell[24] for interpretation of the ferromagnetic behaviour of the *N*-oxyl *N*′-oxides has been extensively discussed.[25] According to this model a spin distribution arising from intramolecular spin polarization of the adjacent atoms leads to alternating positive and negative spin density on the carbon backbone of the radical ligands. In addition, in the radicals, the unpaired electron is known to be localized over the two NO groups with the same spin density on each.[26]

As mentioned above, complex **4** has a shortest intermolecular distance of 2.663(21) Å for NO · · · HC between the neighbouring L^4 radicals. Since these two atoms carry significant spin densities of opposite sign which alternate along the chain, the requirements of the McConnell mechanism are fulfilled. Semi-empirical molecular orbital calculations revealed a strong electronic polarization of NO and CH or OH bonds, indicating the NO groups could act as acceptors and the CH or the OH group as a donor in the hydrogen bonds.[27] A schematic representation of the alternating spin densities for **4** is given in Fig. 8, which also shows the geometrical features relevant to the interaction between the sites carrying the spin density.[25] The positive spin density on the NO(1) sites induces negative spin density on the hydrogen atom of the neighbouring HC(10′) due to a spin polarization, which in turn induces positive spin density on the NO sites of the adjacent molecules caused by the orbital overlap between 1s(H) and π*(NO$^\bullet$), thus we have ↑O(1)–N(2)↑–↓C(7)–↑O(2)N(3)↑–↓C(9)–↑C(12)–H(12)↓ · · · ↑O(1′)–N(2′) and parallel spin alignments of NO sites in **4**.

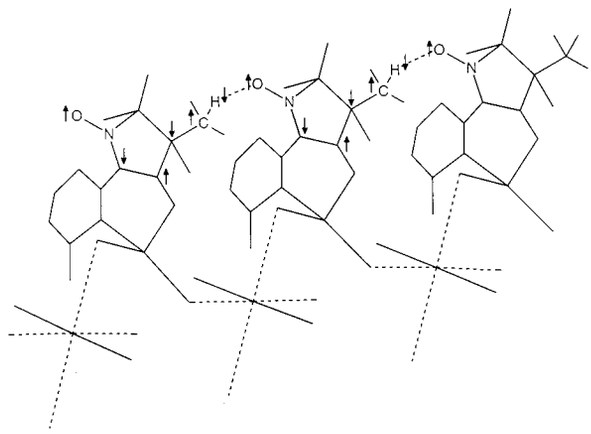

Fig. 8 Schematic drawing of complex **4** showing the alternating spin densities responsible for the ferromagnetic coupling

From the investigations of the structures and cryomagnetic susceptibilities described above, complexes **1**–**3** display a weak antiferromagnetic and **4** a weak ferromagnetic exchange interaction through a superexchange mechanism with intra- and inter-molecular dipole–dipole interaction or spin polarization. The picture emerging from these studies is that the number of $HgBr_2$ moieties, the relative positions of the pyridyl groups, and the intermolecular CH · · · ON contacts in this family of free radicals have a notable influence on their crystal structure packing and structural dimension, thus leading to an important role in the magnetic exchange interactions in the crystals. However, more experimental instances and theoretical calculations are necessary to evaluate more distant interactions.

Acknowledgements

This work is supported by a grant from the National Science Council of Taiwan (NSC86-2113-M032-005).

References

1 A. Caneschi, D. Gatteschi and P. Rey, *Prog. Inorg.*, 1991, **39**, 331.
2 A. Caneschi, P. Chiesi, L. David, F. Ferraro, D. Gatteschi and R. Sessoli, *Inorg. Chem.*, 1993, **32**, 1445.
3 K. Inoue and H. Iwamura, *J. Am. Chem. Soc.*, 1994, **116**, 3173; *Angew. Chem., Int. Ed. Engl.*, 1995, **34**, 927.
4 V. I. Orcharenko, F. L. de Panthou, N. V. Reznikov, P. Rey and R. Z. Sagdeev, *Inorg. Chem.*, 1995, **34**, 2263.
5 K. Awaga, T. Inabe and Y. Maruyama, *Synth. Met.*, 1993, **55**–**57**, 3323; *Chem. Phys. Lett.*, 1990, **190**, 349.
6 K. Inoue and H. Iwamura, *Chem. Phys. Lett.*, 1993, **207**, 551.
7 T. Okuno, T. Otsuka and K. Awaga, *J. Chem. Soc., Chem. Commun.*, 1995, 827.
8 A. Caneschi, F. Ferraro, D. Gatteschi, P. Rey and R. Sessoli, *Inorg. Chem.*, 1990, **29**, 1756, 4217; 1991, **30**, 3162.
9 C. Banelli, A. Caneschi, D. Gatteschi and L. Pardi, *Inorg. Chem.*, 1992, **31**, 741.
10 D. Luneau, G. Risoan, P. Rey, A. Grand, A. Caneschi, D. Gatteschi and J. Laugier, *Inorg. Chem.*, 1993, **32**, 5616.

11 A. Caneschi D. Gatteschi and R. Sessoli, *Inorg. Chim. Acta*, 1991, **184**, 67.
12 F. L. de Panthou, E. Belorizky, R. Calemczuk, D. Luneau, C. Marcenant, E. Ressouche, P. Turek and P. Rey, *J. Am. Chem. Soc.*, 1995, **117**, 11 247.
13 F. L. de Panthou, D. Luneau, J. Laugier and P. Rey, *J. Am. Chem. Soc.*, 1993, **115**, 9095.
14 H. O. Stumpf, L. Ouahab, Y. Pei, D. Grandjean and O. Kahn, *Science*, 1993, **261**, 447.
15 A. Yamaguchi, T. Okuno and K. Awaga, *Bull. Chem. Soc. Jpn.*, 1996, **69**, 875.
16 D. Lanchem and T. W. Wittag, *J. Chem. Soc. C*, 1966, 2300.
17 E. F. Ullmann, L. Call and J. H. Osiecki, *J. Org. Chem.*, 1970, **35**, 3623.
18 O. Kahn, *Molecular Magnetism*, VCH, New York, 1993, p. 3.
19 E. J. Gate, Y. de Page, J. P. Cherland, F. L. Lee and P. S. White, *J. Appl. Crystallogr.*, 1989, **22**, 384.
20 J. W. Hall, W. E. Marsh, R. R. Weller and W. E. Hatfield, *Inorg. Chem.*, 1981, **20**, 1033.
21 J. C. Bonner and M. E. Fischer, *Phys. Rev. A*, 1964, **145**, 640.
22 G. A. Baker, jun., G. S. Rushbrooke and H. E. Gibert, *Phys. Rev.*, 1964, **135**, A1272.
23 K. Yamaguchi, M. Okumura, J. Maki, T. Noro, H. Namimoto, M. Nakano, T. Fueno and K. Nakasuji, *Chem. Phys. Lett.*, 1992, **190**, 353.
24 H. M. McConnell, *J. Chem. Phys.*, 1963, **39**, 1910.
25 J. Cirujeda, M. Mas, E. Molins, F. L. de Panthou, J. Laugier, J. G. Park, C. Paulson, P. Rey, C. Rovira and J. Veciana, *J. Chem. Soc.*, *Chem. Commun.*, 1995, 709; J. Veciana, J. Cirujeda, C. Rovira and J. Vidal-Gancedo, *Adv. Mater.*, 1995, **7**, 221; K. Togashi, R. Imachi, K. Tomioka, H. Tsuboi, Y. Ishida, T. Nogami, N. Takeda and M. Ishikawa, *Bull. Chem. Soc. Jpn.*, 1996, **69**, 2821.
26 K. Awaga, T. Okuno, A. Yamaguchi, M. Hasegawa, T. Inabe, Y. Maruyama and N. Wada, *Phys. Rev. B*, 1994, **49**, 3975.
27 E. Hernandez, M. Mas, E. Molins, C. Rovira and J. Veciana, *Angew. Chem.*, *Int. Ed. Engl.*, 1993, **32**, 882.

Received 14*th July* 1997; *Paper* 7/04999D